Particle Flows for Source Localization in 3-D Using TDOA Measurements

Wenyu Zhang, Mohammad Javad Khojasteh, and Florian Meyer
University of California San Diego, La Jolla, CA
Email: {wez078, m1khojasteh, flmeyer}@ucsd.edu

***Abstract*—Localization using time-difference of arrival (TDOA) has myriad applications, e.g., in passive surveillance systems and marine mammal research. In this paper, we present a Bayesian estimation method that can localize an unknown number of static sources in 3-D based on TDOA measurements. The proposed localization algorithm based on particle flow (PFL) can overcome the challenges related to the highly nonlinear TDOA measurement model, the data association (DA) uncertainty, and the uncertainty in the number of sources to be localized. Different PFL strategies are compared within a unified belief propagation (BP) framework in a challenging multisensor source localization problem. In particular, we consider PFL-based approximation of beliefs based on one or multiple Gaussian kernels with parameters computed using deterministic and stochastic flow processes. Our numerical results demonstrate that the proposed method can correctly determine the number of sources and provide accurate location estimates. The stochastic flow demonstrates greater accuracy compared to the deterministic flow when using the same number of particles.**

I. Introduction

We consider the problem of localizing an unknown number of sources that emit unknown signal waveforms in a three-dimensional (3-D) scenario by passively recording their acoustic or radio signals. Our approach relies on time-difference of arrival (TDOA) measurements that can be extracted, e.g., from the cross-correlation function of multiple spatially separated receivers. TDOA-based localization is particularly relevant in marine mammal research [1] and passive surveillance systems [2]–[4].

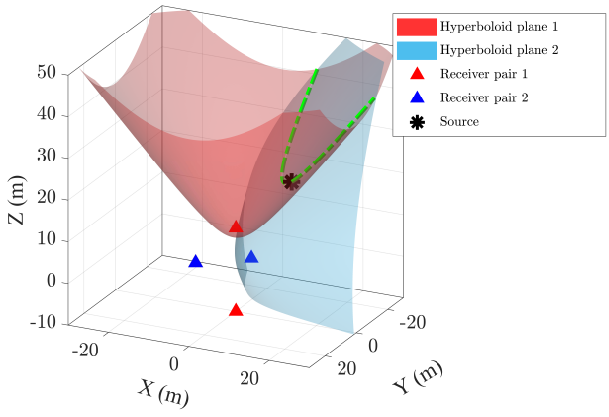

Fig. 1: Source position and hyperboloids resulting from the TDOA measurements of two sensors. Each sensor consists of two receiver pairs. A dashed green line indicates the intersection of the two hyperboloids.

A. Source Localization Using TDOA Measurements

The TDOA measurement of a synchronized receiver pair will lead to 3-D location information on a hyperboloid [5]. The hyperboloids related to a single source provided by multiple receiver pairs are expected to overlap closely with the actual location of the source. Fig. 1 demonstrates the intersected curve (illustrated with the dashed green line) of two hyperboloids defined by 3-D TDOA measurements of two receiver pairs. The localization of multiple sources is more challenging due to data association (DA) uncertainty [6], i.e., multiple TDOA measurements are generated by each receiver pair, but it is unknown which measurement was originated by which source. Furthermore, if signal-to-noise ratio (SNR) is low and in the presence of fading in the propagation paths, the signal of certain sources might be missing at some receivers, and false TDOA measurements not related to a source might be erroneously extracted, which leads to missed detections and false alarms, respectively. Hence, the number of TDOA measurements can differ among receiver pairs. In such a scenario, the number of sources to be localized is unknown, and the state space is high-dimensional and nonlinear. Previous works focused on the simple two-dimensional (2-D) setup [7] and single source localization [8].

For the estimation of an unknown number of sources in the presence of DA uncertainty and nonlinear measurement models, particle-based belief propagation (BP) offers attractive solutions [9], [10]. BP can outperform conventional probabilistic DA methods [11], where the number of sources is known, and multi-hypothesis tracking (MHT) approaches [12], that typically rely on Gaussian approximations of posterior probability density functions (PDFs).

B. Particle Degeneracy

Particle-based BP for multisource localization typically relies on importance sampling [13] for particle-based computations [10]. Following the bootstrap particle filter (BPF) [13], a prior or predicted PDF is typically used as a proposal PDF to draw samples that are then evaluated based on a likelihood function involving the measurements and their statistical model. However, the sampling efficiency of this strategy degrades significantly when the sources' state space has a higher dimension and source PDFs have complicated shapes [14]. In particular, the sampling strategy of the BPF fails in 3-D source localization problems where TDOAs are used as measurements [5], [15]. This is because a very large number of particles is needed to ensure that a sufficient number of them fall into the region of high likelihood for measurement update. For a reasonable number of particles, the low number of particles that fall in the high likelihood region is insufficient to represent the underlying PDF accurately. This effect is typically referred to as "particle degeneracy". To overcome particle degeneracy, the unscented particle filter (UPF) [16] uses the unscented transform to obtain a Gaussian approximation of the posterior PDF to be used as a proposal PDF for sampling. On the other hand, particle flow (PFL) [17], [18] involves migrating a random set of particles from a representation of a prior or predicted PDF to a representation of a posterior PDF density. Particle motion is described by an ordinary differential equation (ODE) or stochastic differential equation (SDE) established by using a log-homotopy function obtained from Bayes' rule in the Fokker–Planck equation [17], [18]. In certain applications, PFL can lead to strongly improved performance and reduced computational complexity compared to conventional

particle-based techniques (see, e.g., [19, Fig. 4]). Different types of PFL have been derived within a deterministic [17], [20] or stochastic [21], [22] framework by solving the ODE and SDE, respectively. Stochastic flows involve a diffusion term with process noise added to particles in the flow. In some applications, their random nature can avoid numerical issues related to implementing the flow in discrete time. These numerical issues are sometimes referred to as stiffness [23] of the flow.

While PFL methods display promising performance, there are generally no theoretical guarantees that an asymptotically optimal representation of the posterior PDF is obtained [24]. Certain PFL can be used as a "measurement-driven" proposal PDF for importance sampling to perform asymptotically optimal estimation. Direct evaluation of the proposal PDF induced by PFL is intractable, and various numerical methods for evaluating this proposal have been considered in the literature. In particular, by focusing on the class of nonlinear Gaussian models, the work in [24] provides numerical approximations of the proposal PDF, generated by PFL within an importance sampling framework using Taylor series expansions. The method proposed in [24] can be computationally demanding, and as an alternative, the authors of [25] utilized auxiliary variables and filters to enhance the performance of importance sampling via PFL more efficiently. The work in [26] extended this framework to the stochastic Gromov's flow. Although the auxiliary methods [25], [26] are computationally less expensive than the method in [24], they still rely on creating an auxiliary variable for each particle individually, which doubles the computational complexity of PFL. Moreover, the choice of Gaussian covariance at each particle is problem-dependent and empirical. The work in [27] improves the estimation accuracy by creating an invertible mapping between the proposal and the prior PDF under the framework of the auxiliary particle filter. However, the invertible mapping is limited to deterministic flows such as exact Daum and Huang (EDH) and localized exact Duam and Huang (LEDH) as proposal PDF. PFL has also been explored in the context of sequential Markov chain Monte Carlo methods for high-dimensional filtering [28], [29].

C. Contribution

In this paper, we aim to solve a challenging 3-D multisource localization based on particle-based BP with DA uncertainty. Within our approach, every pair of receivers is considered a sensor that generates TDOA measurements, and the measurements provided by different sensors are processed sequentially. To address the particle degeneracy of conventional particle-based BP in high-dimensional space, we consider importance sampling based on deterministic and stochastic flow. As deterministic flows, we consider the EDH and the LEDH [17], [20]. In addition, we investigate the stochastic so-called Gromov's flow [22].

The existing auxiliary-based methods [25]–[27] can not be directly applied to the considered static source localization problem, as they rely on an underlying dynamic noise to distinguish the particle from the mean of the auxiliary PDF. We propose a Gaussian mixture model (GMM)-based method [5], [15], which is versatile for static and dynamic source problems. With fewer Gaussian kernels than the particles, the computational complexity can be greatly reduced since flow parameters only have to be computed for each Gaussian kernel. The covariance of each kernel is also analytically updated from the particles. Our method can overcome the challenges related to the highly non-linear TDOA measurement model, the DA uncertainty, and the uncertainty in the number of sources to be localized.

Simulation results confirm that the number of sources can be determined correctly, and accurate location estimates can be obtained when the number of false alarms is low, and the probability of detection is high. The stochastic Gromov's flow achieves the best performance considering the localization accuracy and runtime, which exceeds existing state-of-the-art localization methods. Our simulation result promotes further research into stochastic flow since previous work shows a relatively small improvement in the accuracy of the state estimates [26].

II. System Model

Consider the localization of multiple passive sources using n_r receivers in 3-D in known locations $\boldsymbol{q}^{(k)} = [q_x^{(k)}\, q_y^{(k)}\, q_z^{(k)}]^\mathrm{T}, k = 1, \ldots, n_\mathrm{r}$. The number of sources n_t is unknown and their locations $\boldsymbol{p}^{(j)} = [p_x^{(j)}\, p_y^{(j)}\, p_z^{(j)}]^\mathrm{T}, j = 1, \ldots, n_\mathrm{t}$ are random. Receivers can exchange their received signals and are perfectly synchronized, while the sources emit an unknown waveform at an unknown time.

A. TDOA Measurements

One effective method for acquiring location information of non-synchronized sources with unknown waveforms involves pairwise signal comparison at the receiver end. In this way, for each receiver pair (k, l), the signal of receiver k and the signal of receiver l are correlated, and time delays $z_{kl}^{(m)}$, $m = 1, \ldots, n_{kl}$ related to peaks in the resulting cross-correlation function are extracted. These time delays are referred to as the TDOA measurements [8]. Each TDOA measurement $z_{kl}^{(m)}$ is related to a possible source location $\boldsymbol{p}^{(j)}$ along a hyperboloid surface. For receiver pair (k, l), the random TDOA $z_{kl}^{(m)}$ that was originated by source j is modeled as

$$\begin{aligned} z_{kl}^{(m)} &= \frac{1}{c}\Big(\|\boldsymbol{p}^{(j)} - \boldsymbol{q}^{(k)}\| - \|\boldsymbol{p}^{(j)} - \boldsymbol{q}^{(l)}\|\Big) + v_{kl}^{(m)} \\ &= h_{kl}(\boldsymbol{p}^{(j)}) + v_{kl}^{(m)} \end{aligned} \tag{1}$$

where c is the propagation speed of signal and $v_{kl}^{(m)}$ is the measurement noise which is zero-mean Gaussian with variance σ_v^2 and statistically independent across m and across all (k, l) pairs. Here, we consider that the source signal is received on a single and direct line of sight path. Modeling multipath propagation and refraction is subject to future work. The dependence of a measured TDOA $z_{kl}^{(m)}$ on the location $\boldsymbol{p}^{(j)}$ of the generating source j is described by the likelihood function $f(z_{kl}^{(m)}|\boldsymbol{p}^{(j)})$ that can be directly obtained from (1).

B. Potential Sources (PSs), DA, and Multisource Likelihood Function

For simplicity of notation, we label each receiver pair (k, l) by a single index $s = 1, \ldots, S$, where S is the total number of receiver pairs (a.k.a. sensors). We furthermore denote the two receivers of sensor s by (k_s, l_s) and the number of TDOA measurements at sensor s by $M_s \triangleq n_{k_s l_s}$. Finally, we introduce $\boldsymbol{z}_s \triangleq \left[z_s^{(1)\mathrm{T}} \cdots z_s^{(M_s)\mathrm{T}}\right]^\mathrm{T}$, i.e., the vector of TDOA measurements at sensor s.

With the assumption that one source can generate at most one measurement at a receiver pair and one measurement can originate from at most one source (a.k.a the "the point source assumption" [6], [30], [31]), we can sequentially processing measurements sensor by sensor and formulate the location of an unknown number of sources by introducing augmented PS states $\boldsymbol{y}_s^{(j)} \triangleq \left[\boldsymbol{x}_s^{(j)\mathrm{T}}\, r_s^{(j)}\right]^\mathrm{T}, j = 1, \ldots, J_s$. The number of PSs J_s at sensor s is the maximum possible number of sources that have generated a measurement up to sensor s.

The augmented state of PS $\boldsymbol{y}_s^{(j)}$ incorporates an existence variable $r_s^{(j)} \in \{0, 1\}$ along with PS's state variable $\boldsymbol{x}_s^{(j)}$, which is the source position in our problem, i.e., $\boldsymbol{x}_s^{(j)} \triangleq \boldsymbol{p}^{(j)}$. $r_s^{(j)}$ models the existence/nonexistence of PS j in the sense that PS j exists at sensor s if and only if $r_s^{(j)} = 1$. For nonexistent PSs, i.e., $r_s^{(j)} = 0$, the state $\boldsymbol{x}_s^{(j)}$ is obviously irrelevant. Thus, all PDFs of nonexistent PS

states can be expressed as $f\big(\boldsymbol{x}_s^{(j)}, r_s^{(j)}=0\big) = f_s^{(j)} f_{\mathrm{D}}\big(\boldsymbol{x}_s^{(j)}\big)$, where $f_{\mathrm{D}}\big(\boldsymbol{x}_s^{(j)}\big)$ is an arbitrary "dummy PDF" and $f_s^{(j)} \in [0,1]$ is a constant. For sequential processing of sensors, a new PS is introduced for each of the M_s observed measurements at sensor s, and the total number of PSs is updated as $J_s = J_{s-1} + M_s$. All PSs that have been introduced at previous sensors are referred to as legacy PSs. There are J_{s-1} legacy PSs and M_s new PSs. To distinguish between legacy and new PSs at sensor s, we denote by $\underline{\boldsymbol{y}}_s^{(j)}, j = 1, \ldots, J_{s-1}$ and by $\overline{\boldsymbol{y}}_s^{(m)}, m = 1, \ldots, M_s$ the augmented state of a legacy PS and a new PS states, respectively.

The detection probability denoted as p_{d} is assumed to be constant across sensors. The source represented by PS $j \in \{1, \ldots, J_s\}$ is detected (in the sense that it generates a measurement $z_s^{(m)}$) at sensor s with probability p_{d}. The statistical relationship of a measurement $z_s^{(m)}$ and a detected PS state $\boldsymbol{x}_s^{(j)}$ is described by the conditional PDF $f\big(z_s^{(m)}|\boldsymbol{x}_s^{(j)}\big)$, which is based on the measurement model of the sensor (c.f. (1) for the 3-D TDOA in this work). In multisource localization, measurements are subject to DA uncertainty: it is unknown which measurement originated from which PS, and a measurement may also be clutter, i.e., not originating from any PS. Clutter measurements are modeled by a Poisson point process with mean μ_{c} and PDF $f_{\mathrm{c}}\big(z_s^{(m)}\big)$. With the point source assumption, the association between M_s measurements and J_{s-1} legacy PSs at time k can be modeled by an "source-oriented" DA vector $\boldsymbol{a}_s = \big[a_s^{(1)} \cdots a_s^{(J_{s-1})}\big]^{\mathrm{T}}$. The source-oriented association variable $a_s^{(j)}$ is $m \in \{1, \ldots, M_s\}$ if PS j generates measurement m and zero if PS j is missed by the sensor. For a legacy PS j, the measurement model is represented by the factors

$$q\big(\underline{\boldsymbol{x}}_s^{(j)}, \underline{r}_s^{(j)}=1, a_s^{(j)}; z_s\big) \triangleq \begin{cases} \frac{p_{\mathrm{d}} f(z_s^{(m)}|\underline{\boldsymbol{x}}_s^{(j)})}{\mu_{\mathrm{c}} f_{\mathrm{c}}(z_s^{(m)})}, & a_s^{(j)}=m \in \{1, \ldots, M_s\} \\ 1-p_{\mathrm{d}}, & a_s^{(j)}=0. \end{cases} \tag{2}$$

and $q\big(\underline{\boldsymbol{x}}_s^{(j)}, \underline{r}_s^{(j)}=0, a_s^{(j)}; \boldsymbol{z}_s\big) \triangleq 1(a_s^{(j)})$, where $1(a)$ denotes the indicator function of the event $a = 0$ (i.e., $1(a) = 1$ if $a = 0$ and 0 otherwise) [6]. We also introduce the "measurement-oriented" DA vector $\boldsymbol{b}_s = \big[b_s^{(1)} \cdots b_s^{(M_s)}\big]^{\mathrm{T}}$ to obtain a scalable and efficient message passing algorithm (see [6], [9], [32] for details). The measurement-oriented association variable $b_s^{(m)}$ is $j \in \{1, \ldots, J_{s-1}\}$ if measurement m originated from legacy PS j and zero if it originated from clutter or a newly detected PS. Furthermore, for a new PS, the measurements model is represented by the factors

$$v\big(\overline{\boldsymbol{x}}_s^{(m)}, \overline{r}_s^{(m)}=1, b_s^{(m)}; z_s^{(m)}\big) \triangleq \begin{cases} 0, & b_s^{(m)} \in \{1, \ldots, J_{s-1}\} \\ \frac{f\left(z_s^{(m)}\middle|\overline{\boldsymbol{x}}_s^{(m)}\right)}{\mu_{\mathrm{c}} f_{\mathrm{c}}\left(z_s^{(m)}\right)} \mu_{\mathrm{b}} f_{\mathrm{b}}\big(\overline{\boldsymbol{x}}_s^{(m)}\big), & b_s^{(m)}=0 \end{cases} \tag{3}$$

and $v\big(\overline{\boldsymbol{x}}_s^{(m)}, \overline{r}_s^{(m)}=0, b_s^{(m)}; z_s^{(m)}\big) \triangleq f_{\mathrm{D}}\big(\overline{\boldsymbol{x}}_s^{(m)}\big)$ [6]. In (3), the birth of new PSs is modeled by a Poisson point process with mean μ_{b} and PDF $f_{\mathrm{b}}\big(\overline{\boldsymbol{x}}_s\big)$.

C. Joint Posterior PDF and Problem Formulation

With the previous single PS likelihood, we can obtain the joint posterior PDF of all random variables given the sensors' measurements. In particular, by using common assumptions [6], we obtain the following expression for the joint posterior PDF, i.e.,

$$\begin{aligned} &f\big(\boldsymbol{y}_{0:s}, \boldsymbol{a}_{1:s}, \boldsymbol{b}_{1:s}\big|\boldsymbol{z}_{1:s}\big) \\ &\propto \left(\prod_{j''=1}^{J_0} f\big(\boldsymbol{y}_0^{(j'')}\big)\right) \prod_{s'=1}^{s} \left(\prod_{j'=1}^{J_{s'-1}} f\big(\underline{\boldsymbol{y}}_{s'}^{(j')}\big|\boldsymbol{y}_{s'-1}^{(j')}\big)\right) \\ &\quad \times \left(\prod_{j=1}^{J_{s'-1}} q\big(\underline{\boldsymbol{x}}_{s'}^{(j)}, \underline{r}_{s'}^{(j)}, a_{s'}^{(j)}; \boldsymbol{z}_{s'}\big) \prod_{m'=1}^{M_{s'}} \Psi_{j,m'}\big(a_{s'}^{(j)}, b_{s'}^{(m')}\big)\right) \\ &\quad \times \prod_{m=1}^{M_{s'}} v\big(\overline{\boldsymbol{x}}_{s'}^{(m)}, \overline{r}_{s'}^{(m)}, b_{s'}^{(m)}; z_{s'}^{(m)}\big). \end{aligned} \tag{4}$$

Here, the $f\big(\boldsymbol{y}_0^{(j)}\big)$ are uninformative prior PDF of PS j before any measurement update. These prior PDFs are typically uniformly distributed on a certain region of interest (ROI). The binary indicator function $\Psi_{j,m}\big(a_s^{(j)}, b_s^{(m)}\big)$ in (4) checks association consistency of a pair of source-oriented and measurement-oriented variables $\big(a_s^{(j)}, b_s^{(m)}\big)$ in that $\Psi_{j,m}\big(a_s^{(j)}, b_s^{(m)}\big)$ is zero if $a_s^{(j)} = m, b_s^{(m)} \neq j$ or $b_s^{(m)} = j, a_s^{(j)} \neq m$ and one otherwise (see [6], [9] for details). The state transition PDF $f\big(\underline{\boldsymbol{y}}_s^{(j)}\big|\boldsymbol{y}_{s-1}^{(j)}\big)$ between two sensors is a δ-function $\delta(\underline{\boldsymbol{y}}_s^{(j)} - \boldsymbol{y}_{s-1}^{(j)})$.

With the joint posterior PDF presented in (4), we formulate the detection and localization problem we want to solve. We consider the problem of simultaneous detection and localization of an unknown number of static sources based on all measurements $\boldsymbol{z}_{1:S}$ collected by a total number of S multiple receiver pairs (sensors). Source detection is performed by comparing the existence probability $p\big(r_S^{(j)}=1\big|\boldsymbol{z}_{1:S}\big)$ with a threshold P_{th}, i.e., PS $j \in \{1, \ldots, J_S\}$ is declared to exist if $p\big(r_S^{(j)} = 1\big|\boldsymbol{z}_{1:S}\big) > P_{\mathrm{th}}$. Note that $p\big(r_S^{(j)} = 1\big|\boldsymbol{z}_{1:S}\big) = \int f\big(\boldsymbol{x}_S^{(j)}, r_S^{(j)} = 1\big|\boldsymbol{z}_{1:S}\big)\,\mathrm{d}\boldsymbol{x}_S^{(j)}$. For existent PSs, state estimation is performed by calculating the minimum mean-square error (MMSE) estimate [33] as

$$\hat{\boldsymbol{x}}_S^{(j)} \triangleq \int \boldsymbol{x}_S^{(j)} f\big(\boldsymbol{x}_S^{(j)}\big|r_S^{(j)}=1, \boldsymbol{z}_{1:S}\big)\,\mathrm{d}\boldsymbol{x}_S^{(j)} \tag{5}$$

where $f\big(\boldsymbol{x}_S^{(j)}\big|r_S^{(j)} = 1, \boldsymbol{z}_{1:S}\big) = f\big(\boldsymbol{x}_S^{(j)}, r_S^{(j)} = 1\big|\boldsymbol{z}_{1:S}\big)/p\big(r_S^{(j)} = 1\big|\boldsymbol{z}_{1:S}\big)$.

Both source detection and estimation require the marginal posterior PDF $f\big(\boldsymbol{x}_S^{(j)}, r_S^{(j)}\big|\boldsymbol{z}_{1:S}\big) \triangleq f\big(\boldsymbol{y}_S^{(j)}\big|\boldsymbol{z}_{1:S}\big)$, $j \in \{1, \ldots, J_S\}$. Using the Markovian property of the joint posterior PDF, we can update the marginal posterior PDF $f\big(\boldsymbol{x}_s^{(j)}, r_s^{(j)}\big|\boldsymbol{z}_{1:s}\big)$ by processing TDOA measurements $\boldsymbol{z}_s$ sequentially across sensors $s \in \{1, \ldots, S\}$.

D. Message Passing Operations

Typically, calculating $f\big(\boldsymbol{x}_s^{(j)}, r_s^{(j)}\big|\boldsymbol{z}_{1:s}\big), s = 1, \ldots, S$ by directly marginalization over (4) is infeasible due to a large number of parameters. As in [6], [10], we approximate the marginal posterior PDF by performing a loopy BP on the factor graph in Fig. 2 and passing messages forward across sensor indexes. More specifically, let's consider the message passing for a single sensor s. The belief computed for sensor $s-1$, i.e., $\tilde{f}\big(\boldsymbol{x}_{s-1}^{(j)}, r_{s-1}^{(j)}\big) \approx f\big(\boldsymbol{x}_{s-1}^{(j)}, r_{s-1}^{(j)}\big|\boldsymbol{z}_{1:s-1}\big)$, is directly used as prior information for computations at sensor s since a Dirac delta function describes state-transition between sensor indexes. For computations related to sensor s, this "prior belief" is denoted as $\alpha_s\big(\underline{\boldsymbol{y}}_s^{(j)}\big)$. For legacy PSs, the messages $\beta_s^{(j)}\big(a_s^{(j)}\big)$ passed from factor nodes $q\big(\underline{\boldsymbol{x}}_s^{(j)}, \underline{r}_s^{(j)}, a_s^{(j)}; \boldsymbol{z}_s\big)$ to variable nodes $a_s^{(j)}$ are calculated as

$$\begin{aligned} \beta_s^{(j)}\big(a_s^{(j)}\big) = &\int q\big(\underline{\boldsymbol{x}}_s^{(j)}, 1, a_s^{(j)}; \boldsymbol{z}_s\big)\alpha_s^{(j)}\big(\underline{\boldsymbol{x}}_s^{(j)}, 1\big)\mathrm{d}\underline{\boldsymbol{x}}_s^{(j)} \\ &+ 1\big(a_s^{(j)}\big)\alpha_{\mathrm{n},s}^{(j)}. \end{aligned} \tag{6}$$

where $\alpha_{\mathrm{n},s}^{(j)} = \int \alpha_s^{(j)}\big(\underline{\boldsymbol{x}}_s^{(j)}, \underline{r}_s^{(j)} = 0\big)\mathrm{d}\underline{\boldsymbol{x}}_s^{(j)}$. For new PSs, messages $\xi_k^{(m)}\big(b_k^{(m)}\big)$ are calculated similarly (see [6, Section IX]). Now, probabilistic DA is performed by using the iterative BP-based algorithm [6, Section IX-A3] with input messages $\beta_s^{(j)}\big(a_s^{(j)}\big)$, $j \in \{1, \ldots, J_{s-1}\}$ and $\xi_s^{(m)}\big(b_s^{(m)}\big)$, $m \in \{1, \ldots, M_s\}$. After convergence, corresponding output messages $\kappa_s^{(j)}\big(a_s^{(j)}\big)$, $j \in \{1, \ldots, J_{s-1}\}$

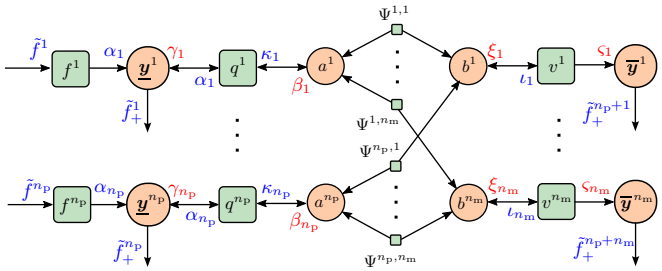

Fig. 2: Factor graph for message passing of an unknown number of sources at a single sensor s, corresponding to the propagation of the joint PDF (4). Messages calculated using PFL are depicted in red. These messages are calculated based on messages depicted in blue. The following short notations are used: $n_{\mathrm{m}} \triangleq M_s$, $n_{\mathrm{p}} \triangleq J_{s-1}$, $\underline{\boldsymbol{y}}^j \triangleq \underline{\boldsymbol{y}}_s^{(j)}$, $\overline{\boldsymbol{y}}^m \triangleq \overline{\boldsymbol{y}}_s^{(m)}$, $\boldsymbol{a}^j \triangleq \boldsymbol{a}_s^{(j)}$, $\boldsymbol{b}^m \triangleq \boldsymbol{b}_s^{(m)}$, $f^j \triangleq f\big(\underline{\boldsymbol{y}}_s^{(j)}\big|\underline{\boldsymbol{y}}_{s-1}^{(j)}\big)$, $q^j \triangleq q\big(\underline{\boldsymbol{x}}_s^{(j)}, \underline{r}_s^{(j)}, a_s^{(j)}; \boldsymbol{z}_s\big)$, $v^m \triangleq v\big(\overline{\boldsymbol{x}}_s^{(m)}, \overline{r}_s^{(m)}, b_s^{(m)}; \boldsymbol{z}_s^{(m)}\big)$, $\Psi^{j,m} \triangleq \Psi_{j,m}\big(a_s^{(j)}, b_s^{(m)}\big)$, $\gamma_j \triangleq \gamma_s^{(j)}\big(\underline{\boldsymbol{y}}_s^{(j)}\big)$, $\beta_j \triangleq \beta_s^{(j)}\big(a_s^{(j)}\big)$, $\xi_m \triangleq \xi_s^{(m)}\big(b_s^{(m)}\big)$, $\varsigma_m \triangleq \varsigma_s^{(m)}\big(\overline{\boldsymbol{y}}_s^{(m)}\big)$, $\tilde{f}^j \triangleq \tilde{f}\big(\underline{\boldsymbol{y}}_{s-1}^{(j)}\big)$, $\alpha_j \triangleq \alpha_s\big(\underline{\boldsymbol{y}}_s^{(j)}\big)$, $\kappa_j \triangleq \kappa_s^{(j)}\big(a_s^{(j)}\big)$, $\iota_m \triangleq \iota_s^{(m)}\big(b_s^{(m)}\big)$, and $\tilde{f}_+^j \triangleq \tilde{f}\big(\underline{\boldsymbol{y}}_s^{(j)}\big)$.

and $\iota_s^{(m)}\big(b_s^{(m)}\big)$, $m \in \{1, \ldots, M_s\}$ are available for legacy PSs and new PSs, respectively.

Next, a "measurement update" step is performed. For legacy PSs, messages $\gamma_s^{(j)}\big(\underline{\boldsymbol{x}}_s^{(j)}, \underline{r}_s^{(j)}\big)$ passed from $q\big(\underline{\boldsymbol{x}}_s^{(j)}, \underline{r}_s^{(j)}, a_s^{(j)}; \boldsymbol{z}_s\big)$ to $\underline{\boldsymbol{y}}_s^{(j)}$ are calculated as

$$\gamma_s^{(j)}\big(\underline{\boldsymbol{x}}_s^{(j)}, 1\big) = \sum_{a_s^{(j)}=0}^{M_s} q\big(\underline{\boldsymbol{x}}_s^{(j)}, 1, a_s^{(j)}; \boldsymbol{z}_s\big)\kappa_k^{(j)}\big(a_s^{(j)}\big) \tag{7}$$

and $\gamma_s^{(j)}\big(\underline{\boldsymbol{x}}_s^{(j)}, 0\big) = \gamma_s^{(j)} = \kappa_s^{(j)}(0)$. Finally, beliefs are calculated to approximate the posterior PDFs of PSs. In particular, for legacy PSs, beliefs $\tilde{f}\big(\underline{\boldsymbol{x}}_s^{(j)}, \underline{r}_s^{(j)}\big)$ approximating $f\big(\underline{\boldsymbol{x}}_s^{(j)}, \underline{r}_s^{(j)}\big|\boldsymbol{z}_{1:s}\big)$ are obtained as

$$\tilde{f}\big(\underline{\boldsymbol{x}}_s^{(j)}, 1\big) = \frac{1}{\underline{C}_s^{(j)}}\alpha_s^{(j)}\big(\underline{\boldsymbol{x}}_s^{(j)}, 1\big)\gamma_s^{(j)}\big(\underline{\boldsymbol{x}}_s^{(j)}, 1\big) \tag{8}$$

and $\tilde{f}\big(\underline{\boldsymbol{x}}_s^{(j)}, 0\big) = \underline{f}_s^{(j)} f_{\mathrm{D}}\big(\underline{\boldsymbol{x}}_s^{(j)}\big)$ with $\underline{f}_s^{(j)} = \alpha_{\mathrm{n},s}^{(j)}\gamma_s^{(j)}/\underline{C}_s^{(j)}$. The constant $\underline{C}_s^{(j)}$ is given by $\underline{C}_s^{(j)} \triangleq \int \alpha_s^{(j)}\big(\underline{\boldsymbol{x}}_s^{(j)}, 1\big)\,\gamma_s^{(j)}\big(\underline{\boldsymbol{x}}_s^{(j)}, 1\big)\mathrm{d}\underline{\boldsymbol{x}}_s^{(j)} + \alpha_{\mathrm{n},s}^{(j)}\gamma_s^{(j)}$.

E. Particle Approximation of Selected Messages

Note that neither (6) (7) nor (2) (3) have a parametric solution in general due to complex integral as well as non-linearity of measurement model (1). As a result, we propose to approximate those messages and likelihood functions by Monte Carlo importance sampling. Let's take (6) as an example. If we can approximate the message $\alpha_s^{(j)}\big(\underline{\boldsymbol{x}}_s^{(j)}, 1\big)$ by a set of weighted particles $\big\{\big(\underline{\boldsymbol{x}}_0^{(j,i)}, \underline{w}_0^{(j,i)}\big)\big\}_{i=1}^{N_{\mathrm{s}}}$ in that $\sum_{i=1}^{N_{\mathrm{s}}} \underline{w}_0^{(j,i)} \approx \int \alpha_s^{(j)}\big(\underline{\boldsymbol{x}}_s^{(j)}, 1\big)\mathrm{d}\underline{\boldsymbol{x}}_s^{(j)}$, then we can approximate (6) as

$$\tilde{\beta}_s^{(j)}\big(a_s^{(j)} = a\big) = \sum_{i=1}^{N_{\mathrm{s}}} q\big(\underline{\boldsymbol{x}}_0^{(j,i)}, 1, a; \boldsymbol{z}_s\big)\underline{w}_0^{(j,i)} + 1(a)\tilde{\alpha}_{\mathrm{n},s}^{(j)} \tag{9}$$

where $\tilde{\alpha}_{\mathrm{n},s}^{(j)} = 1 - \sum_{i=1}^{N_{\mathrm{s}}} \underline{w}_0^{(j,i)}$.

Note that in (9) we sample from $\alpha_s^{(j)}\big(\underline{\boldsymbol{x}}_s^{(j)}, 1\big)$, which can be seen as the prior PDF of legacy PS with index j. However, note that $q\big(\underline{\boldsymbol{x}}_s^{(j)}, \underline{r}_s^{(j)}; 1, a_s^{(j)}; z_s\big)$ incorporates the measurement likelihood $f\big(z_s^{(m)}\big|\underline{\boldsymbol{x}}_s^{(j)}\big)$ (c.f. (2)), which suffers from particle degeneracy similarly to BPF [14]. The underlying inefficiency of sampling from the prior PDF is that few samples fall into the region of high likelihood of $f\big(z_s^{(m)}\big|\underline{\boldsymbol{x}}_s^{(j)}\big)$ (e.g., the hyperboloid at the first sensor or the intersected curve of two hyperboloids at the second sensor in Fig. 1 [5]), which makes a poor approximation of the target message $\beta_s^{(j)}\big(a_s^{(j)}\big)$. Similarly, also the messages $\gamma_s^{(j)}\big(\underline{\boldsymbol{y}}_s^{(j)}\big)$ based on (2) as well as $\xi_s^{(m)}\big(b_s^{(m)}\big)$ and $\varsigma_s^{(m)}\big(\overline{\boldsymbol{y}}_s^{(m)}\big)$ based on (3) are affected by particle degeneracy). We propose to use PFL to overcome particle degeneracy.

III. Review of Deterministic and Stochastic PFLs

In this section, we review deterministic and stochastic PFLs and discuss relevant approaches to drive PFL-based proposal PDFs.

A. Deterministic PFL: EDH and LEDH Flow

The Bayesian PFL [17], [18] tries to define a continuous mapping $\Phi : \boldsymbol{X}_0 \times [0,1] \to \boldsymbol{X}_1$ to migrate particles sampled from the topological space of prior PDF $\boldsymbol{x}_0^{(i)} \sim \boldsymbol{X}_0$ to the topological space of posterior PDF $\boldsymbol{x}_1^{(i)} \sim \boldsymbol{X}_1$. The process is time-dependent w.r.t. a pseudo-time $\lambda \in [0,1]$.

Let $f(\boldsymbol{x})$ be the prior PDF, $h(\boldsymbol{x}) = f(\boldsymbol{z}|\boldsymbol{x})$ be the likelihood function (e.g. (1) for TDOA model). Following Bayes' rule, a log-homotopy function is introduced [17], [18] as

$$\phi(\boldsymbol{x}, \lambda) = \log f(\boldsymbol{x}) + \lambda \log h(\boldsymbol{x}). \tag{10}$$

Note that the homotopy function defines a continuous and smooth deformation from $\phi(\boldsymbol{x}, 0) = \log f(\boldsymbol{x})$ to $\phi(\boldsymbol{x}, 1) = \log \pi(\boldsymbol{x})$, where $\pi(\boldsymbol{x}) = f(\boldsymbol{x})f(\boldsymbol{z}|\boldsymbol{x})$ is the unnormalized posterior PDF. The drift of the flow $\boldsymbol{\zeta}(\boldsymbol{x}, \lambda) = \mathrm{d}\boldsymbol{x}/\mathrm{d}\lambda$ is calculated by solving an ODE and hence used to drive the dynamics of particles deterministically. Since the drift depends on $\boldsymbol{x}$, the direct integral over λ from 0 to 1 typically has no analytical solution. The Euler method is commonly used for numerical implementation, where particle migration is performed by calculating $\boldsymbol{\zeta}(\boldsymbol{x}, \lambda)$ at N_λ discrete values of λ, i.e., $0 = \lambda_0 < \lambda_1 < \ldots < \lambda_{N_\lambda} = 1$. First, N_{s} particles $\big\{\boldsymbol{x}_0^{(i)}\big\}_{i=1}^{N_{\mathrm{s}}}$ are drawn from $f(\boldsymbol{x})$. Next, these particles are migrated sequentially across discrete pseudo time steps $l \in \{1, \ldots, N_\lambda\}$, i.e.,

$$\boldsymbol{x}_{\lambda_l}^{(i)} = \boldsymbol{x}_{\lambda_{l-1}}^{(i)} + \boldsymbol{\zeta}(\boldsymbol{x}_{\lambda_{l-1}}^{(i)}, \lambda_l)(\lambda_l - \lambda_{l-1}) \tag{11}$$

for all $i \in \{1, \ldots, N_{\mathrm{s}}\}$. In this way, particles $\{\boldsymbol{x}_1^{(i)}\}_{i=1}^{N_{\mathrm{s}}}$ representing the posterior PDF $\pi(\boldsymbol{x})$ are obtained.

If $\log f(\boldsymbol{x})$ and $\log h(\boldsymbol{x})$ are polynomials (e.g., $f(\boldsymbol{x})$ and $h(\boldsymbol{x})$ are Gaussians or in another exponential family), the drift term can be solved exactly [20]. In particular, let us consider a Gaussian prior $f(\boldsymbol{x}) = \mathcal{N}(\boldsymbol{x}; \boldsymbol{\mu}_0, \boldsymbol{P})$ with mean $\boldsymbol{\mu}_0$ and covariance matrix $\boldsymbol{P}$ as well as a linear measurement model $\boldsymbol{z} = \boldsymbol{H}\boldsymbol{x} + \boldsymbol{v}$. Here, the measurement noise $\boldsymbol{v}$ is zero-mean Gaussian with covariance matrix $\boldsymbol{R}$. The EDH flow [20] is given by

$$\boldsymbol{\zeta}_{\mathrm{d}}(\boldsymbol{x}, \lambda) = \boldsymbol{A}(\lambda)\boldsymbol{x} + \boldsymbol{b}(\lambda) \tag{12}$$

where

$$\boldsymbol{A}(\lambda) = -\frac{1}{2}\boldsymbol{P}\boldsymbol{H}^{\mathrm{T}}(\lambda\boldsymbol{H}\boldsymbol{P}\boldsymbol{H}^{\mathrm{T}} + \boldsymbol{R})^{-1}\boldsymbol{H}$$

$$\boldsymbol{b}(\lambda) = (\boldsymbol{I} + 2\lambda\boldsymbol{A}(\lambda))\big[(\boldsymbol{I} + \lambda\boldsymbol{A}(\lambda))\boldsymbol{P}\boldsymbol{H}^{\mathrm{T}}\boldsymbol{R}^{-1}\boldsymbol{z} + \boldsymbol{A}(\lambda)\boldsymbol{\mu}_0\big].$$

For nonlinear measurement models $\boldsymbol{z} = \boldsymbol{h}(\boldsymbol{x}) + \boldsymbol{v}$, a suboptimal linearization step is employed, i.e. $\tilde{\boldsymbol{H}}_{l-1} = \frac{\partial \boldsymbol{h}}{\partial \boldsymbol{x}}\big|_{\boldsymbol{x}=\boldsymbol{\mu}_{\lambda_{l-1}}}$ at a current mean $\boldsymbol{\mu}_{\lambda_{l-1}}$. This mean is propagated in parallel to the particles $\{\boldsymbol{x}_{\lambda_{l-1}}^{(i)}\}_{i=1}^{N_{\mathrm{s}}}$ by using (11). Alternatively, linearization can be performed at each particle, i.e., at $\tilde{\boldsymbol{H}}_{l-1}^{(i)} = \frac{\partial \boldsymbol{h}}{\partial \boldsymbol{x}}\big|_{\boldsymbol{x}=\boldsymbol{x}_{\lambda_{l-1}}^{(i)}}$ where $\tilde{\boldsymbol{A}}^{(i)}(\lambda)$ and $\tilde{\boldsymbol{b}}^{(i)}(\lambda)$ are computed for each particle respectively. This

is known as the LEDH flow. The EDH flow is computationally much faster than the LEDH flow since it only calculates a single pair of global flow parameters $\boldsymbol{A}$ and $\boldsymbol{b}$. However, the PDF of particles after the flow still follows a Gaussian PDF. (Note that the flow in (12) can be seen as a sequence of affine transformations applied to the Gaussian prior.) On the other hand, the LEDH flow provides particles that follow an arbitrary probability PDF since each particle follows an individual affine transform. However, since a different pair of flow parameters is computed for each particle, the computational complexity of the LEDH flow is N_s times higher than EDH flow.

B. Stochastic PFL Gromov's Flow

The migration of particles corresponding to (10) can alternatively be describe by a SDE [22], i.e.,

$$\mathrm{d}\boldsymbol{x} = \boldsymbol{\zeta}_\mathrm{s}(\boldsymbol{x},\lambda)\mathrm{d}\lambda + \mathrm{d}\boldsymbol{w}_\lambda \tag{13}$$

where $\boldsymbol{\zeta}_\mathrm{s}(\boldsymbol{x},\lambda) \in \mathbb{R}^N$ is the stochastic drift and $\mathrm{d}\boldsymbol{w}$ is the N-dimensional standard Brownian motion with positive-definite diffusion matrix $\mathrm{d}\boldsymbol{w}\,\mathrm{d}\boldsymbol{w}^\mathrm{T} = \boldsymbol{Q}(\lambda) \in \mathbb{R}^{N\times N}$ [22]. The stochastic PFL outperforms deterministic PFL for improving the transient dynamics. In some applications, their random nature can avoid numerical issues, referred to as stiffness of the flow [23]), related to implementing the flow using discrete values of pseudo-time λ.

One of the most popular stochastic flow with a closed-form solution is Gromov's flow, where

$$\boldsymbol{\zeta}_\mathrm{g}(\boldsymbol{x},\lambda) = -\left(\nabla_{\boldsymbol{x}}\nabla_{\boldsymbol{x}}^\mathrm{T}\phi\right)^{-1}\nabla_{\boldsymbol{x}}\log h \tag{14}$$

with the following solution for diffusion matrix

$$\boldsymbol{Q}_\mathrm{g} = -\left(\nabla_{\boldsymbol{x}}\nabla_{\boldsymbol{x}}^\mathrm{T}\phi\right)^{-1}\left(\nabla_{\boldsymbol{x}}\nabla_{\boldsymbol{x}}^\mathrm{T}\log h\right)\left(\nabla_{\boldsymbol{x}}\nabla_{\boldsymbol{x}}^\mathrm{T}\phi\right)^{-1}. \tag{15}$$

One of the advantages of Gromov's flow is that it provides an unbiased estimate of the state [34].

Given Gaussian prior and linear approximation of measurement model as in the EDH flow, we have $\nabla_{\boldsymbol{x}}\log h = \boldsymbol{H}^\mathrm{T}\boldsymbol{R}^{-1}(\boldsymbol{z}-\boldsymbol{H}\boldsymbol{x})$, $\nabla_{\boldsymbol{x}}\nabla_{\boldsymbol{x}}^\mathrm{T}\log h = -\boldsymbol{H}^\mathrm{T}\boldsymbol{R}^{-1}\boldsymbol{H}$ and $\nabla_{\boldsymbol{x}}\nabla_{\boldsymbol{x}}^\mathrm{T}\phi = -\boldsymbol{P}^{-1} - \lambda\boldsymbol{H}^\mathrm{T}\boldsymbol{R}^{-1}\boldsymbol{H}$. Then we can rewrite (14) and (15) as

$$\boldsymbol{\zeta}_\mathrm{g}(\boldsymbol{x},\lambda) = \left(\boldsymbol{P}^{-1} + \lambda\boldsymbol{H}^\mathrm{T}\boldsymbol{R}^{-1}\boldsymbol{H}\right)^{-1}\boldsymbol{H}^\mathrm{T}\boldsymbol{R}^{-1}(\boldsymbol{z}-\boldsymbol{H}\boldsymbol{x}) \tag{16}$$

$$\boldsymbol{Q}_\mathrm{g} = (\boldsymbol{P}^{-1}+\lambda\boldsymbol{H}^\mathrm{T}\boldsymbol{R}^{-1}\boldsymbol{H})^{-1}(\boldsymbol{H}^\mathrm{T}\boldsymbol{R}^{-1}\boldsymbol{H})(\boldsymbol{P}^{-1}+\lambda\boldsymbol{H}^\mathrm{T}\boldsymbol{R}^{-1}\boldsymbol{H})^{-1}. \tag{17}$$

We can still parameterize the drift similarly as EDH as

$$\boldsymbol{\zeta}_\mathrm{g}(\boldsymbol{x},\lambda) = \boldsymbol{A}_\mathrm{g}(\lambda)\boldsymbol{x} + \boldsymbol{b}_\mathrm{g}(\lambda)$$

where the parameters of the flow are given by

$$\boldsymbol{A}_\mathrm{g}(\lambda) = -\left(\boldsymbol{P}^{-1} + \lambda\boldsymbol{H}^\mathrm{T}\boldsymbol{R}^{-1}\boldsymbol{H}\right)^{-1}\boldsymbol{H}^\mathrm{T}\boldsymbol{R}^{-1}\boldsymbol{H}$$

$$\boldsymbol{b}_\mathrm{g}(\lambda) = \left(\boldsymbol{P}^{-1} + \lambda\boldsymbol{H}^\mathrm{T}\boldsymbol{R}^{-1}\boldsymbol{H}\right)^{-1}\boldsymbol{H}^\mathrm{T}\boldsymbol{R}^{-1}\boldsymbol{z}.$$

C. PFL as Proposal PDF

Although PFL methods display very promising characteristics, due to approximations related to the discretization of pseudo time λ, they are unable to provide an asymptotically optimal representation of the posterior PDF $\pi(\boldsymbol{x})$. However, for asymptotically optimal estimation, PFL methods can be used to provide samples and a proposal PDF $q(\boldsymbol{x})$ for importance sampling [13].

Direct evaluation of the proposal PDF $q(\boldsymbol{x})$ related to PFL is complicated by the fact that a closed-form expression of $q(\boldsymbol{x})$ is unavailable. For the numerical evaluation of $q(\boldsymbol{x}_1^{(i)})$, $i = 1,\ldots,N_\mathrm{s}$, the following two approaches can be employed: i) deriving an invertible mapping from the prior to the posterior PDF [27] and ii) developing a Gaussian proposal PDF where mean and covariance are updated sequentially based on flow equations [25].

As presented in [27], for an affine deterministic flow, there exists an invertible mapping $\theta : f(\boldsymbol{x}_0^{(i)}) \to \pi(\boldsymbol{x}_1^{(i)})$ with linear operator θ. This motivates a proposal PDF given by $q(\boldsymbol{x}_1^{(i)}) = f(\boldsymbol{x}_0^{(i)})/\tilde{\theta}$ where the approximate mapping factor $\tilde{\theta}$ is defined as

$$\tilde{\theta} = \prod_{l=1}^{N_\lambda}\left|\det\left[\boldsymbol{I} + (\lambda_l - \lambda_{l-1})\,\tilde{\boldsymbol{A}}(\lambda_l)\right]\right|. \tag{18}$$

Deriving an invertible mapping for stochastic flows remains an open research problem. As an alternative, following the second approach discussed above, we develop a Gaussian proposal PDF based on stochastic flow, as discussed next.

IV. BP-Based Source Localization With Embedded Stochastic PFL

In this section, we develop a GMM representation of posterior PDFs based on stochastic PFL and demonstrate how it can be incorporated into our BP framework for source localization.

A. Proposal Evaluation and GMM-Based Representation

Proposal evaluation based on deterministic flow within a GMM representation of beliefs has been presented in [5]. Here, we adapt this strategy to the use of a stochastic flow within the GMM representation. The primary motivation for using a GMM representation is that it can represent non-Gaussian beliefs with potentially complicated shapes. Being able to model complicated beliefs is important in multisensor localization and tracking problems where the dimension of the individual sensor measurements is lower than the dimension of object positions as, e.g., in the scenario shown in Fig. 1. Moreover, by leveraging a mixture of Gaussian kernels to model beliefs, PFL can be performed for each Gaussian kernel in parallel.

Let's first consider a single Gaussian prior $f(\boldsymbol{x}) = \mathcal{N}(\boldsymbol{x};\boldsymbol{\mu}_0,\boldsymbol{\Sigma}_0 \triangleq \boldsymbol{P})$. For discrete time $0 = \lambda_0 < \cdots < \lambda_{N_\lambda} = 1$, we can update the mean and covariance by making using of the stochastic flow in (13), i.e.,

$$\boldsymbol{\mu}_{\lambda_l} = \boldsymbol{\mu}_{\lambda_{l-1}} + \boldsymbol{\zeta}_\mathrm{g}(\boldsymbol{\mu}_{\lambda_{l-1}},\lambda_l)(\lambda_l - \lambda_{l-1}) \tag{19}$$

$$\begin{aligned}\boldsymbol{\Sigma}_{\lambda_l} = {}&[\boldsymbol{I} + (\lambda_l - \lambda_{l-1})\boldsymbol{A}_\mathrm{g}(\lambda_l)]\boldsymbol{\Sigma}_{\lambda_{l-1}}[\boldsymbol{I} + (\lambda_l - \lambda_{l-1})\boldsymbol{A}_\mathrm{g}(\lambda_l)]^\mathrm{T}\\ &+ (\lambda_l - \lambda_{l-1})\boldsymbol{Q}_\mathrm{g}(\lambda_l)\end{aligned} \tag{20}$$

for $l = 1,\ldots,N_\lambda$. We can then evaluate the proposal at the particles as $q(\boldsymbol{x}_1^{(i)}) = \mathcal{N}(\boldsymbol{x}_1^{(i)};\boldsymbol{\mu}_1,\boldsymbol{\Sigma}_1)$.

Next, we utilize (19) and (20) in a GMM model. More precisely, instead of sampling $\{\boldsymbol{x}_0^{(i)}\}_{i=1}^{N_\mathrm{s}}$ from a Gaussian prior $f(\boldsymbol{x}) = \mathcal{N}(\boldsymbol{x};\boldsymbol{\mu}_0,\boldsymbol{\Sigma}_0)$, we model the prior as GMM with N_k kernels, i.e., $f(\boldsymbol{x}) \propto \sum_{k=1}^{N_\mathrm{k}}\mathcal{N}(\boldsymbol{x};\boldsymbol{\mu}_0^{(k)},\boldsymbol{\Sigma}_0^{(k)})$. This mixture representation makes it possible to approximate arbitrary PDFs. In particular, it enables to closely approximate localization information on a hyperboloid as provided by TDOA measurements. Then for each kernel k, we sample $\{\boldsymbol{x}_0^{(i,k)}\}_{i=1}^{N_\mathrm{p}}$ from $\mathcal{N}(\boldsymbol{x};\boldsymbol{\mu}_0^{(k)},\boldsymbol{\Sigma}_0^{(k)})$ and use $\left\{\{\boldsymbol{x}_0^{(i,k)}\}_{i=1}^{N_\mathrm{p}}\right\}_{k=1}^{N_\mathrm{k}}$ as the particle set. Hence, the equivalent particle number is $N_\mathrm{p}\times N_\mathrm{k}$. For the stochastic flow and using the Gaussian solution, the proposal at particles for each kernel is $q(\boldsymbol{x}_1^{(i,k)}) = \mathcal{N}(\boldsymbol{x}_1^{(i,k)};\boldsymbol{\mu}_1^{(k)},\boldsymbol{\Sigma}_1^{(k)})$.

The methodology for updating kernels from particles within the GMM framework is discussed in [5]. In particular, one flow is performed for each Gaussian kernel in the GMM, and the resulting particles are used to compute updated Gaussian parameters. The number of Gaussian kernels in our proposed GMM algorithm is much smaller than the number of particles, i.e., $N_\mathrm{k} << N_\mathrm{p}$. As

a result, compared to [25], [26], much fewer flow parameters have to be computed, which results in a significantly reduced computational complexity.

B. BP With Embedded Stochastic PFL

We finally discuss how to approximate BP messages in Section II-E based on stochastic PFL. Let's still use (6) as an example. In addition, for simplicity, let's assume that the message $\alpha_s^{(j)}(\underline{\boldsymbol{x}}_s^{(j)}, 1)$ is represented by a single Gaussian $\mathcal{N}(\underline{\boldsymbol{x}}_s^{(j)}; \boldsymbol{\mu}_s^{(j)}, \boldsymbol{\Sigma}_s^{(j)})$ and approximate existent probability $\tilde{\alpha}_{\mathrm{e},s}^{(j)} \approx \int \alpha_s^{(j)}(\underline{\boldsymbol{x}}_s^{(j)}, 1)\mathrm{d}\underline{\boldsymbol{x}}_s^{(j)}$. We can then directly sample from the this Gaussian to obtain a set of weighted particles $\{(\underline{\boldsymbol{x}}_s^{(j,i)}, \underline{w}_s^{(j,i)})\}_{i=1}^{N_\mathrm{s}}$ with $\underline{w}_s^{(j,i)} = \tilde{\alpha}_{\mathrm{e},s}^{(j)}/N_\mathrm{s}$ as an alternative representation of $\alpha_s^{(j)}(\underline{\boldsymbol{x}}_s^{(j)}, 1)$. To improve the sampling efficiency related to the computation of the messages $\beta_s^{(j)}(a_s^{(j)} = m), m \in \{1, \ldots, M_s\}$, we migrate the samples $\{\underline{\boldsymbol{x}}_s^{(j,i)}\}_{i=1}^{N_\mathrm{s}}$ using stochastic PFL. In particular, we perform M_s parallel flows, one for each measurement $z_s^{(m)}$, $m \in \{1, \ldots, M_s\}$. After the M_s parallel flows have been completed, we computed M_s sets of particles, i.e., $\{\underline{\boldsymbol{x}}_{s,m}^{(j,i)}\}_{i=1}^{N_\mathrm{s}}$, $m \in \{1, \ldots, M_s\}$. Then for $a = 1, \ldots, M_s$, we can rewrite (9) as

$$\tilde{\beta}_s^{(j)}(a_s^{(j)} = a) = \sum_{i=1}^{N_\mathrm{s}} q(\underline{\boldsymbol{x}}_{s,a}^{(j,i)}, 1, a; \boldsymbol{z}_s)\underline{w}_{s,a}^{(j,i)} + 1(a)\,\tilde{\alpha}_{\mathrm{n},s}^{(j)} \tag{21}$$

with $\tilde{\alpha}_{\mathrm{e},s}^{(j)} = 1 - \tilde{\alpha}_{\mathrm{n},s}^{(j)}$ (cf. (9)). Here, particle weights are computed as $\underline{w}_{s,a}^{(j,i)} = \mathcal{N}(\underline{\boldsymbol{x}}_s^{(j)}; \boldsymbol{\mu}_s^{(j)}, \boldsymbol{\Sigma}_s^{(j)}) / \mathcal{N}(\underline{\boldsymbol{x}}_s^{(j)}; \boldsymbol{\mu}_{s,a}^{(j)}, \boldsymbol{\Sigma}_{s,a}^{(j)})\, \underline{w}_s^{(j,i)}$ where the parameters of the Gaussian proposal, i.e., $\boldsymbol{\mu}_{s,a}^{(j)}$ and $\boldsymbol{\Sigma}_{s,a}^{(j)}$ are obtained following (19) and (20).

If the message $\alpha_s^{(j)}(\underline{\boldsymbol{x}}_s^{(j)}, 1)$ is represented by a GMM, (21) can be rewrite as

$$\tilde{\beta}_s^{(j)}(a_s^{(j)} = a) = \frac{1}{N_\mathrm{k}} \sum_{k=1}^{N_\mathrm{k}} \sum_{i=1}^{N_\mathrm{p}} q(\underline{\boldsymbol{x}}_{s,a}^{(j,i,k)}, 1, a; \boldsymbol{z}_s)\underline{w}_{\mathrm{s},a}^{(j,i,k)} + 1(a)\,\tilde{\alpha}_{\mathrm{n},s}^{(j)}$$

where $\underline{w}_{\mathrm{s},a}^{(j,i,k)}$ is computed based on the Gaussian proposal resulting from the flow performed for measurement $m = a$ and Gaussian kernel k. Following a similar flow-based processing, further messages for legacy and new PSs, namely $\gamma_s^{(j)}(\underline{\boldsymbol{y}}_s^{(j)})$, $\xi_s^{(m)}(b_s^{(m)})$ and $\varsigma_s^{(m)}(\overline{\boldsymbol{y}}_s^{(m)})$ can also be efficiently computed. As discussed in the next section, by embedding PFL, BP message passing can provide accurate estimation results in challenging nonlinear and high-dimensional problems even with a relatively moderate number of particles.

V. Implementation Aspects and Results

In this section, we test our proposed BP algorithm with GMM PFL embedded for sequential processing of 3-D TDOA measurements in a 3-D multisource localization problem. To the best of our knowledge, the GMM PFL algorithm hasn't been tested for a challenging task to detect and localize multiple sources appearing at the same time in a 3-D space. As expected from the discussion in Section III-B and IV-A, we will demonstrate that the GMM Gromov's flow outperforms the other reference methods. The baseline method under comparison is the bootstrap particle filter, wherein the prior message is utilized for particle sampling (abbreviated as "PM" for later notation). Apart from the Gromov's flow, we also implement GMM with deterministic flows embedded as a reference, such as the EDH flow [20] (abbreviated as "EDH") and the LEDH flow (abbreviated as "LEDH").

A. Simulation Parameters

In our simulations the sources are randomly placed on a ROI of $[-1000\,\mathrm{m}, 1000\,\mathrm{m}] \times [-1000\,\mathrm{m}, 1000\,\mathrm{m}] \times [-1000\,\mathrm{m}, 1000\,\mathrm{m}]$. The source-originated TDOAs $\mathsf{z}_{kl}^{(m)}$ at receiver pair (k, l) are distributed according to (1) with a standard deviation of $\sigma_z = 0.001\mathrm{m}/c$ for the noise $v_{kl}^{(m)}$, where c is the propagation speed of signal in the environment. We set $c = 1500$m/s to model acoustic propagation in water. The clutter PDF $f_\mathrm{c}(z_s^{(m)})$ at receiver pair (k, l) is uniform on $\|\boldsymbol{q}^{(k)} - \boldsymbol{q}^{(l)}\|/c$ following Poisson point process with mean $\mu_\mathrm{c} = 1$. Six receivers are located at the center of each face of the ROI cube. The probability of detection p_d is set to 0.95. The number of receiver pairs S is 9.

For a single realization, Fig. 3 shows simulation results for a scenario with three static sources. For each source, the GMM consists of $N_\mathrm{k} = 100$ kernels; each is importance sampled using EDH flow. The particle size is $\underline{N}_\mathrm{p} = 1000$ for previously detected sources and $\overline{N}_\mathrm{p} = 1000$ for newly detected sources at the current sensor. In Fig. 3, particles are shown in different colors to represent the spatial PDFs of the PSs j with the existence probabilities $f(r_s^{(j)} = 1|\boldsymbol{z}_{1:s})$ larger than $P_\mathrm{th} = 0.5$ (hence regarded as existence) by sensor s, i.e., $f(\boldsymbol{x}_s^{(j)}|r_s^{(j)} = 1, \boldsymbol{z}_{1:s})$ for $s = 1, 2, 4, 9$ in Fig. 3(a)-(d) respectively. Some observations regarding the evolution of particles between sensor pairs are as follows.

- The first receiver pair ($s = 1$) has one missed detection and one clutter measurement. Two sets of particles (pink and orange) meet the true locations of two sources, while the other set (grey) corresponds to the clutter. Spatial PDFs are approximated hyperbolas in Y-Z and X-Z planes. The particles in the X-Y plane have not been updated effectively since the first sensor pair is at unfavorable locations for localization in that plane.
- The second receiver pair ($s = 2$) has no missed detection. The two components with the highest existence probabilities are the legacy components generated from the measurements of the first receiver pair (pink and orange). The third existing component (blue) is regarded as the third source, which is newly detected. Note that the clutter source shown as a grey particle in the first receiver pair no longer exists since there is no measurement matching that clutter in the current receiver pair.
- The number of sources has been correctly determined after the first two sensors. After the fourth sensor had been updated, spatial PDFs of the three sources were still multimodal but more concentrated around the true source locations than the $s = 2$ result. Their spatial PDFs have modes that correspond to the intersection points of the hyperbolas related to previous measurements and current measurements.
- After the update step has been performed for all receiver pairs, all three existing components have a single mode well localized around the actual locations of the three sources.

B. Results

To investigate how the performance of our method depends on GMM parameters and sampling size, we simulated scenarios with different numbers of kernels and particles per kernel.

Table I shows the mean optimum subpattern assignment (OSPA) error [35] (with a cutoff threshold at 50) and runtime per run for different algorithms and system parameters. Not that for PM, we have $N_\mathrm{p} = N_\mathrm{s}$. All methods are simulated on a single core of an Intel Xeon Gold 5222 CPU. The runtime is averaged over 100 Monte Carlo runs, each with five static sources randomly placed in ROI. It can be seen that the PM performed the worst in terms of OSPA error. This is expected since the PM is based on bootstrap sampling, which suffers particle degeneracy in the considered scenario. In contrast, the implementation based on deterministic flow, such as EDH, can achieve a much smaller OSPA error with much fewer particles and reasonable runtime. The implementation based on the LEDH has

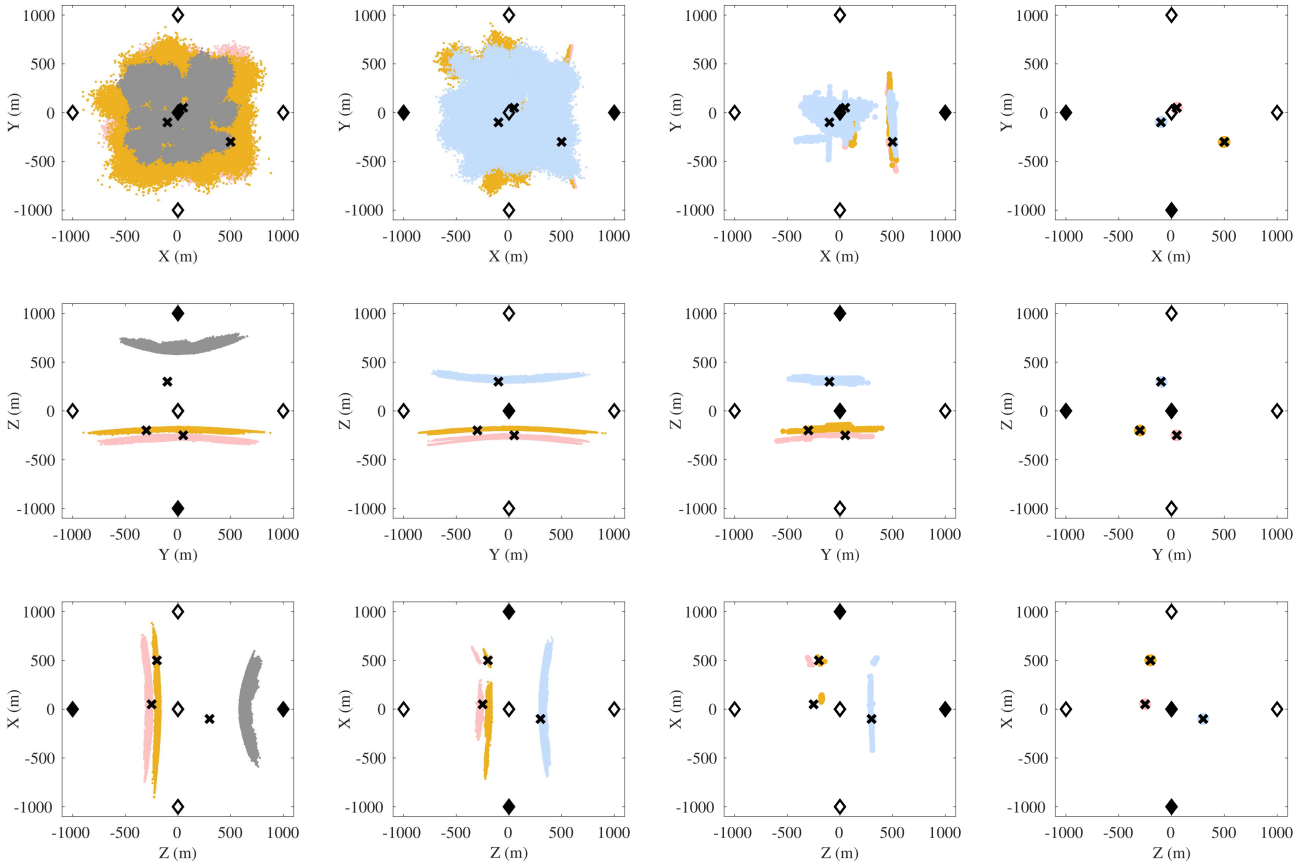

Fig. 3: Particle-based representation after the EDH flow of the spatial PDFs by GMM model. There exist three signal sources in a 3-D environment with clutters, and the state is sequentially filtered by sensor: (a) $s = 1$, (b) $s = 2$, (c) $s = 4$, and (d) $s = 9 = n_{\mathrm{s}}$. Filled diamonds indicate the locations of receivers involved in the current update step; the locations of other receivers are indicated by empty diamonds. X-marks indicate the sources' ground truth positions.

a slightly better performance than EDH, but the runtime has been increased significantly (see ID 3 vs. ID 4). Further increasing particle size $\underline{N}_{\mathrm{p}}$ and $\overline{N}_{\mathrm{p}}$ can improve the localization accuracy (see ID 5 and 6 vs. ID 3) but limited to a bottleneck with OSPA around 20. The implementation based on stochastic flow such as Gromov's flow can significantly reduce the OSPA error compared with EDH flow using same particle size (see ID 7 vs. ID 3, and ID 8 vs. ID 5), whereas three times in runtime. Overall, Gromov's flow with parameter setting as ID 7 is best among all tested methods with a trade-off between localization accuracy and runtime.

ID	Method	$(N_{\mathrm{k}}, \underline{N}_{\mathrm{p}}, \overline{N}_{\mathrm{p}})$	OSPA	Runtime(s)
1	PM	$(-, 2\mathrm{e}6, 2\mathrm{e}6)$	43.90	75.4
2	PM	$(-, 1\mathrm{e}7, 1\mathrm{e}7)$	32.07	443.3
3	EDH	$(100, 500, 30)$	25.17	196.9
4	LEDH	$(100, 500, 30)$	23.23	4934.2
5	EDH	$(100, 3\mathrm{e}3, 500)$	20.57	379.6
6	EDH	$(100, 1\mathrm{e}4, 1\mathrm{e}4)$	19.58	2586.8
7	Gromov	$(100, 500, 30)$	10.43	568.8
8	Gromov	$(100, 3\mathrm{e}3, 500)$	8.75	1356.1

TABLE I: Simulated mean OSPA error and runtime per run for different algorithms and system parameters.

The statistical box plot [36] of the 100 OSPA samples for each algorithm is shown in Fig. 4 for further comparison. Here, the box with a blue boundary has its lower and upper bound as the first and third quartile of the 100 samples, respectively. The vertical range of the box is the interquartile range (IQR). The red line in the box is the median. The black lines that extend from the box are the expected variation as either the minimum/maximum value of the samples or the whiskers (i.e., $1.5\times$ IQR extension from the box boundary) if there are outliers. If the second case, the outliers are marked as red '+'s. Notably, the median of Gromov's flow is much lower than that of EDH flow, which means it has a much higher chance of detecting all five static sources.

VI. Conclusion

In this paper, we propose a BP method for localizing an unknown number of sources in 3-D based on TDOA measurements. Our method relies on GMMs to represent approximate marginal posterior PDFs, called beliefs, with complicated shapes for accurate localization in 3-D using a nonlinear measurement model. By passing BP messages, represented as weighted particles, over a factor graph, our method can simultaneously detect and localize an unknown number of sources in the presence of DA uncertainty, false alarms, and clutter. The novelty of our approach lies in leveraging stochastic PFL for the efficient update of GMM parameters of beliefs. The considered stochastic PFL, referred to as Gromov's flow, achieves the best

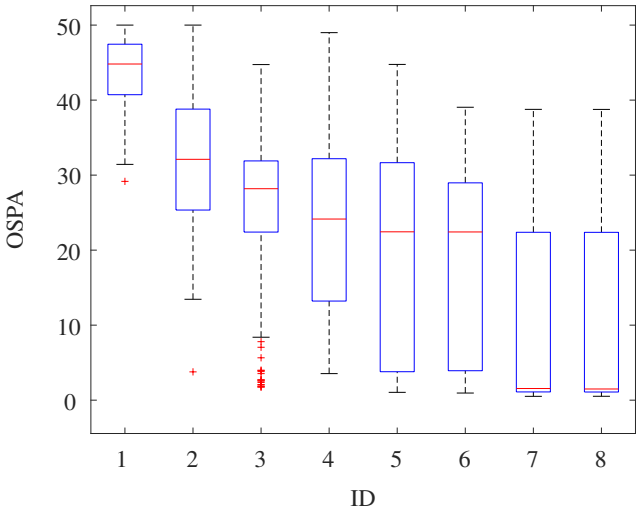

Fig. 4: Statistics of the OSPA error for different algorithms. Each column corresponds to the algorithm with the same ID as in Table I.

accuracy-complexity tradeoff in numerical experiments, compared to previously considered deterministic flows. Future research includes information fusion of multiple types of measurement models with PFL and the development of novel stochastic PFLs with improved transient dynamics. Modeling unresolved measurements [37], combining PFL with BP-based track-before-detect methods [38], or introducing deep learning techniques to refine the BP solution [39] are also possible venues for future research.

Acknowledgment

The material presented in this work was supported by Qualcomm Innovation Fellowship 492866 and by the Office of Naval Research under Grant N00014-23-1-2284.

References

[1] J. Jang, F. Meyer, E. R. Snyder, S. M. Wiggins, S. Baumann-Pickering, and J. A. Hildebrand, "Bayesian detection and tracking of odontocetes in 3-d from their echolocation clicks," *J. Acoust. Soc. Am.*, vol. 153, no. 5, p. 2690–2705, May 2023.

[2] A. Quazi, "An overview on the time delay estimate in active and passive systems for target localization," *IEEE Trans. Acoust., Speech, and Signal Process.*, vol. 29, no. 3, pp. 527–533, Jun. 1981.

[3] Y. Huang, J. Benesty, G. W. Elko, and R. M. Mersereati, "Real-time passive source localization: A practical linear-correction least-squares approach," *IEEE Trans. Speech and Audio Process.*, vol. 9, no. 8, pp. 943–956, Nov. 2001.

[4] A. Tesei, F. Meyer, and R. Been, "Tracking of multiple surface vessels based on passive acoustic underwater arrays," *J. Acoust. Soc. Am.*, vol. 147, no. 2, pp. EL87–EL92, Feb. 2020.

[5] W. Zhang and F. Meyer, "Multisensor multiobject tracking with improved sampling efficiency," *IEEE Trans. Signal Process.*, vol. 72, pp. 2036–2053, 2024.

[6] F. Meyer, T. Kropfreiter, J. L. Williams, R. A. Lau, F. Hlawatsch, P. Braca, and M. Z. Win, "Message passing algorithms for scalable multitarget tracking," *Proc. IEEE*, vol. 106, no. 2, pp. 221–259, Feb. 2018.

[7] F. Meyer, A. Tesei, and M. Z. Win, "Localization of multiple sources using time-difference of arrival measurements," in *Proc. IEEE ICASSP-17*, Mar. 2017, pp. 3151–3155.

[8] F. Gustafsson and F. Gunnarsson, "Positioning using time-difference of arrival measurements," in *Proc. IEEE ICASSP-03*, vol. 6, Hong Kong, China, Apr. 2003, pp. 553–556.

[9] J. L. Williams and R. Lau, "Approximate evaluation of marginal association probabilities with belief propagation," *IEEE Trans. Aerosp. Electron. Syst.*, vol. 50, no. 4, pp. 2942–2959, Oct. 2014.

[10] F. Meyer, P. Braca, P. Willett, and F. Hlawatsch, "A scalable algorithm for tracking an unknown number of targets using multiple sensors," *IEEE Trans. Signal Process.*, vol. 65, no. 13, pp. 3478–3493, Jul. 2017.

[11] Y. Bar-Shalom and X. T. P. K. Willet and, *Tracking and Data Fusion: A Handbook of Algorithms*. Storrs, CT, USA: Yaakov Bar-Shalom, 2011.

[12] D. B. Reid, "An algorithm for tracking multiple targets," *IEEE Trans. Autom. Control*, vol. 24, no. 6, pp. 843–854, Dec. 1979.

[13] M. S. Arulampalam, S. Maskell, N. Gordon, and T. Clapp, "A tutorial on particle filters for online nonlinear/non-Gaussian Bayesian tracking," *IEEE Trans. Signal Process.*, vol. 50, no. 2, pp. 174–188, Feb. 2002.

[14] P. Bickel, B. Li, and T. Bengtsson, "Sharp failure rates for the bootstrap particle filter in high dimensions," in *Pushing the Limits of Contemporary Statistics: Contributions in Honor of Jayanta K. Ghosh*, vol. 3. Beachwood, OH, USA: Inst. Math. Statist., 2008, pp. 318–329.

[15] W. Zhang and F. Meyer, "Graph-based multiobject tracking with embedded particle flow," in *Proc. IEEE RadarConf-21*, Atlanta, GA, USA, May 2021.

[16] R. van der Merwe, A. Doucet, N. de Freitas, and E. Wan, "The unscented particle filter," in *Proc. NIPS-00*, Denver, CO, USA, Dec. 2000, pp. 584–590.

[17] F. Daum and J. Huang, "Nonlinear filters with log-homotopy," in *Proc. SPIE-07*, Aug. 2007, pp. 423–437.

[18] ——, "Nonlinear filters with particle flow induced by log-homotopy," in *Proc. SPIE-09*, May 2009, pp. 76–87.

[19] N. Moshtagh, J. Chan, and M. Chan, "Homotopy particle filter for ground-based tracking of satellites at GEO," in *Proc. AMOS-16*, Maui, HI, Sep. 2016, pp. 1–6.

[20] F. Daum, J. Huang, and A. Noushin, "Exact particle flow for nonlinear filters," in *Proc. SPIE-10*, Apr. 2010, pp. 92–110.

[21] F. Daum and J. Huang, "Particle flow with non-zero diffusion for nonlinear filters," in *Proc. SPIE-13*, May 2013, pp. 226–238.

[22] F. Daum, J. Huang, and A. Noushin, "New theory and numerical results for Gromov's method for stochastic particle flow filters," in *Proc. FUSION-18*, 2018, pp. 108–115.

[23] L. Dai and F. Daum, "On the design of stochastic particle flow filters," *IEEE Trans. Aerosp. Electron. Syst.*, vol. 59, no. 3, pp. 2439–2450, 2023.

[24] P. Bunch and S. Godsill, "Approximations of the optimal importance density using Gaussian particle flow importance sampling," *J. Amer. Statist. Assoc.*, vol. 111, no. 514, pp. 748–762, Aug. 2016.

[25] Y. Li, L. Zhao, and M. Coates, "Particle flow auxiliary particle filter," in *Proc. IEEE CAMSAP-15*, Cancun, Mexico, Dec. 2015, pp. 157–160.

[26] S. Pal and M. Coates, "Particle flow particle filter using Gromov's method," in *Proc. IEEE CAMSAP-19*, Guadeloupe, France, Dec. 2019, pp. 634–638.

[27] Y. Li and M. Coates, "Particle filtering with invertible particle flow," *IEEE Trans. Signal Process.*, vol. 65, no. 15, pp. 4102–4116, Aug. 2017.

[28] M. A. Khan, A. De Freitas, L. Mihaylova, M. Ulmke, and W. Koch, "Bayesian processing of big data using log homotopy based particle flow filters," in *Proc. IEEE SDF-17*, 2017.

[29] Y. Li and M. Coates, "Sequential MCMC with invertible particle flow," in *Proc. IEEE ICASSP-17*, 2017, pp. 3844–3848.

[30] Y. Bar-Shalom, P. K. Willett, and X. Tian, *Tracking and Data Fusion: A Handbook of Algorithms*. Storrs, CT: Yaakov Bar-Shalom, 2011.

[31] R. Mahler, *Statistical Multisource-Multitarget Information Fusion*. Norwood, MA: Artech House, 2007.

[32] F. Meyer and J. L. Williams, "Scalable detection and tracking of geometric extended objects," *IEEE Trans. Signal Process.*, vol. 69, pp. 6283–6298, 2021.

[33] H. V. Poor, *An Introduction to Signal Detection and Estimation*, 2nd ed. New York: Springer-Verlag, 1994.

[34] D. F. Crouse, "Particle flow filters: biases and bias avoidance," in *Proc. FUSION-19*, Ottawa, Canada, July 2019, pp. 1–8.

[35] D. Schuhmacher, B.-T. Vo, and B.-N. Vo, "A consistent metric for performance evaluation of multi-object filters," *IEEE Trans. Signal Process.*, vol. 56, no. 8, pp. 3447–3457, 2008.

[36] J. Tukey, *Exploratory Data Analysis*. Addison-Wesley, 1977.

[37] W. Koch and G. Van Keuk, "Multiple hypothesis track maintenance with possibly unresolved measurements," *IEEE Trans. Aerosp. Electron. Syst.*, vol. 33, no. 3, pp. 883–892, 1997.

[38] M. Liang, T. Kropfreiter, and F. Meyer, "A BP method for track-before-detect," *IEEE Signal Process. Lett.*, vol. 30, pp. 1137–1141, 2023.

[39] M. Liang and F. Meyer, "Neural enhanced belief propagation for multiobject tracking," *IEEE Trans. Signal Process.*, vol. 72, pp. 15–30, 2024.